KLOE-2

KLOE-2 Collaboration - LNF Group

D. Babusci, G. Bencivenni, C. Bloise, F. Bossi, G. Capon (Ass.), P. Ciambrone, F. Curciarello (PostDoc), E. Dané (Art. 23), E. De Lucia (Resp.), A. De Santis (Art.36), P. De Simone, D. Domenici, G. Felici, P. Fermani (PostDoc), G. Fortugno (Tec.), S. Giovannella, X. Kang (PostDoc), M. Martini (Ass)*, S. Miscetti, E. Perez del Rio (Art.36), P. Santangelo, F. Sborzacchi (Tec.), M. Berlowski (PostDoc), G. Venanzoni.

In collaboration with "LNF-SEA"
P. Albicocco, A. Balla, M. Beretta, M. Carletti, S. Ceravolo, G. Corradi, U. Denni, A. Frani, M. Gatta, R. Lenci, G. Papalino, B. Ponzio

**Also Dipartimento di Scienze e Tecnologie applicate, "Guglielmo Marconi" University, Rome, Italy*

1 DAΦNE Operation and KLOE-2 Run

Data taking campaign in 2017 proceeded with good efficiency and good performance for both accelerator and detector, exploiting continuous detector status monitoring and data quality assessment with benchmark channels. Run-III started in September 2016 with the intermediate milestone of additional 2 fb^{-1} integrated luminosity delivered by July 2017 which has been reached, and Run-IV started in September 2017 with the final goal of acquiring at least 5 fb^{-1} by the end of March 2018. A total integrated luminosity of about 1.8 fb^{-1} has been acquired during 2017 (Fig.1).

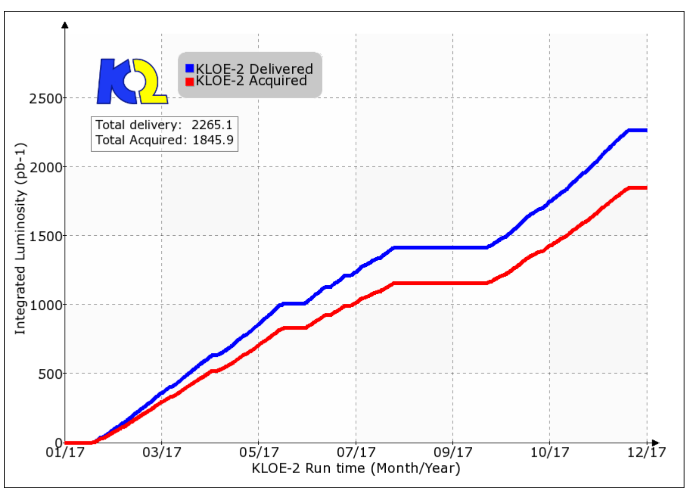

Figure 1: 2017 Integrated luminosity: the blue curve shows DAΦNE delivered luminosity and the red curve KLOE-2 acquired luminosity respectively.

2 Data Quality and Analysis

Event Classification Counters are constantly monitored to provide fast feedback during data taking. Some of the counters monitored over the period from April to July 2017 are shown as an example in Fig.2, exhibiting good stability.

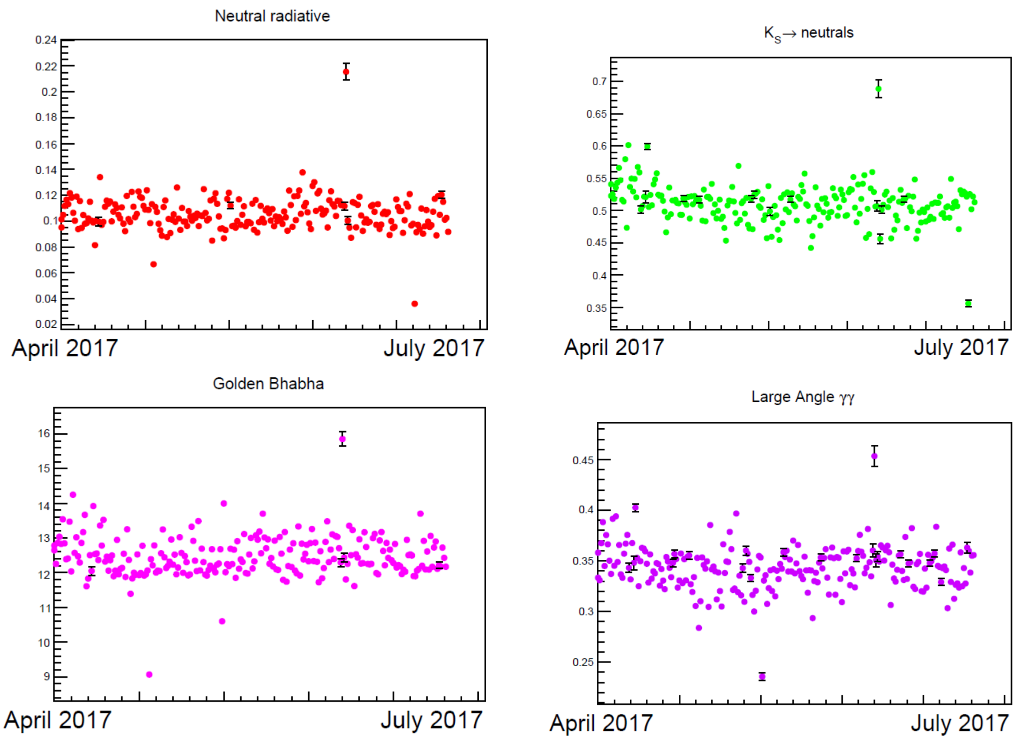

Figure 2: Event Classification Counters for the data period from April to July 2017: neutral radiative (Top Left), $K_S \to$ neutrals (Top Right), golden Bhabha scattering (Bottom Left) and large-angle $\gamma\gamma$ (Bottom Right) streams.

To assess data quality several benchmark channels have been reconstructed and analyzed. Fully neutral processes like $\phi \to \eta\gamma$, with both $\eta \to 3\pi^0$ and $\eta \to \gamma\gamma$, have been used to monitor the calorimeter performance. Decays with charged secondaries like $\phi \to \pi^+\pi^-\pi^0$ and $K_{L,S} \to \pi^+\pi^-$ have been used to monitor the tracking performance.
In order to investigate Dark Matter mediator scenarios and ALPs (Axion Like Particles) not excluded by present limits, a new stream of data has been added to the Event Classification to store events selected by a new Single Photon Trigger (SPHOT).

2.1 Analysis exploiting the Inner Tracker

The first set of alignment and calibration parameters obtained with cosmic-ray muon data has been used to validate the integrated tracking and vertexing algorithms using both Inner Tracker (IT) and Drift Chamber (DC) information, exploiting the Kalman filter technique. Bhabha scattering events and decays close to the interaction point (IP) seen by both DC and IT detectors have been used for benchmark studies. Preliminary results have been obtained using both $\phi \to \pi^+\pi^-\pi^0$ and $K_S \to \pi^+\pi^-$ decays.

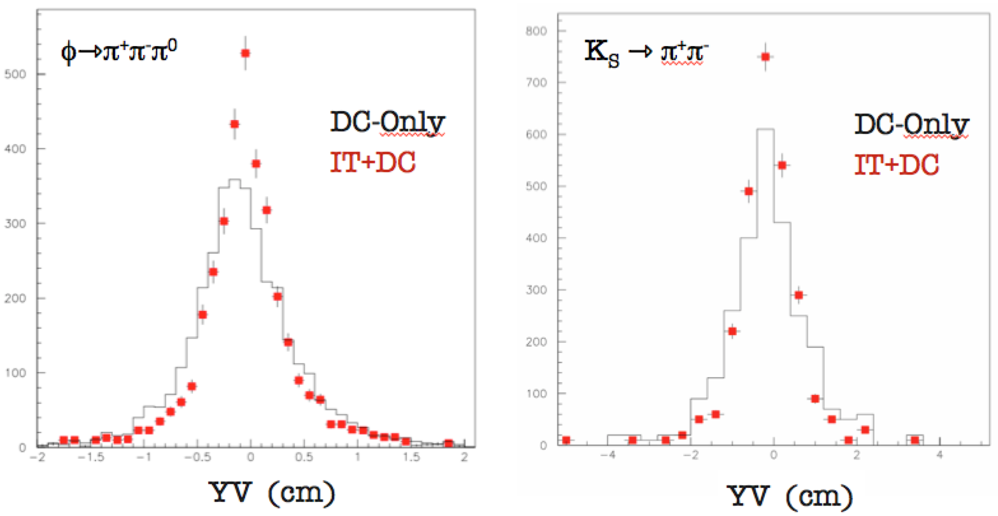

Figure 3: The distribution of the y coordinate of the reconstructed vertex position of $\phi \to \pi^+\pi^-\pi^0$ (Left) and $K_S \to \pi^+\pi^-$ (Right) decays: comparison between DC-only (solid line) and integrated IT+DC reconstruction (points).

A good figure of merit of the vertex resolution close to the IP is represented by the distribution of the y coordinate YV of the reconstructed vertex position of $\phi \to \pi^+\pi^-\pi^0$ decays, due to the negligible beam size contribution along the vertical direction, tens of μm. Fig.3 left shows the improvement in the YV distribution of $\phi \to \pi^+\pi^-\pi^0$ decays, obtained using the integrated tracking. Fitting the distribution with a double Gaussian function, the 3 mm standard deviation of the narrow component obtained with DC-only reconstruction is reduced to about 2 mm with the integrated reconstruction.

Similar results have been obtained with $K_S \to \pi^+\pi^-$ decays (Fig.3 right) in which the YV distribution is the convolution of beam size, vertex resolution and K_S lifetime. The total $\sigma_{\rm DC} \sim$ 1 cm of the double Gaussian fit to the YV distribution obtained with DC-only reconstruction is reduced to $\sigma_{\rm IT+DC} \sim 0.7$ cm using the integrated reconstruction [1].

Preliminary results on the fit to the K_S proper time distribution in τ_S units, obtained with the first integrated tracking version, show a total resolution improvement from 1.4 τ_S DC-only to 1 τ_S already using the first set of IT alignment and calibration parameters [1]. Improvement are expected with the refined alignment and calibration and further integrated tracking optimization.

2.2 Analysis exploiting the HET

Two tagger stations (HET) for the detection of electrons and positrons from photon fusion are installed in the Roman Pots at the exit of the bending dipoles, eleven meters from the IP. Several studies have been performed to establish detector performance during data taking.

A precise measurement of the HET time resolution and the offset between stations has been obtained from the fit with Gaussian functions of the delay between hits in the electron and positron arm (Fig. 4 left) in the interval $|\Delta T| < 20$ ns (13 bunch crossings), distribution dominated by e^+/e^- scattered particles coming from independent beam crossings.

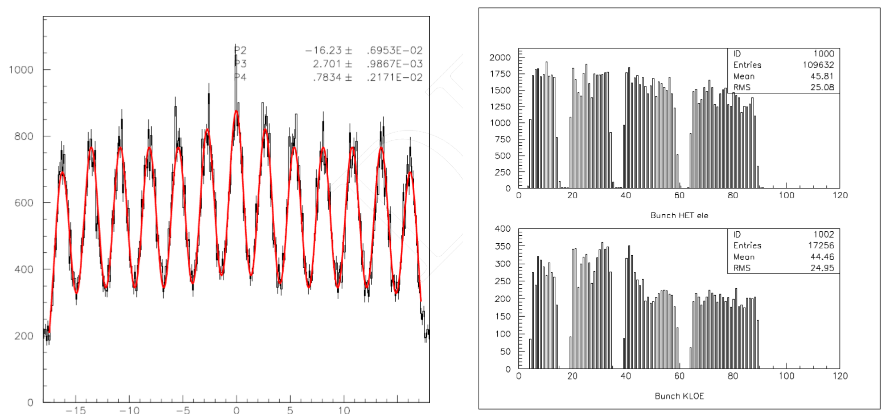

Figure 4: Left: hit delay distribution between the HET stations. Right: DAΦNE bunch structure as measured by the electron HET station (top) and by KLOE (bottom).

The HET hit time structure closely reproduces DAΦNE bunch structure observed with KLOE, by selecting Bhabha scattering events (Fig. 4 right), and the rate timeline strictly follows the luminosity timeline as measured by the KLOE detector (Fig. 5). Measurements (blue

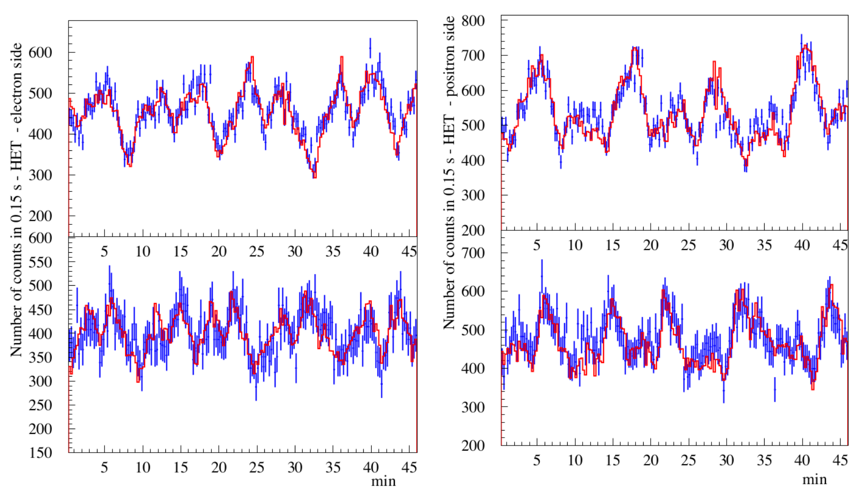

Figure 5: Timeline of the counting rate of the e^- (Left) and e^+ (Right) HET stations. Top and bottom plots refer to different data taking periods.

points) are compared with the expectation (red line) given by an intra-bunch scattering term ($\propto I^2_{\mathrm{e,p}}$) contributing together with a term proportional to the instantaneous luminosity.

The analysis on π^0 production from $\gamma\gamma$ scattering has been progressing, studying detector trigger efficiency and cluster reconstruction in the calorimeter. The energy of tagged final state photons E_γ ~70 MeV is close to trigger threshold E_{thr} ~50 MeV. Fig. 6-left shows the trigger efficiency as function of the cluster energy, as obtained using Bhabha scattering events. The fit to data gives the expected trigger threshold, at 52 MeV. The global trigger efficiency for near-to-rest

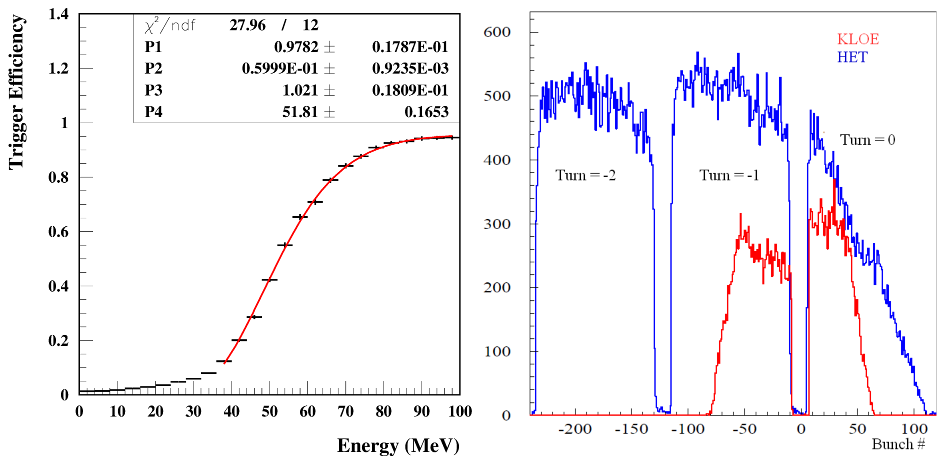

Figure 6: Left: Barrel trigger efficiency as function of the cluster energy. The red curve is the fit performed with the convolution of the threshold function with a Gaussian. Right: overlapping of the KLOE and HET acquisition windows.

π^0's is 65%, given by the measurement of the probability for 70 MeV photons to exceed the energy threshold ($\sim$80%). The KLOE calorimeter energy, momentum and time resolution for 70 MeV photons is crucial for analysis cuts and associated efficiency. The resolutions in energy, longitudinal and transverse momentum, and time have been measured with a sub-sample of radiative Bhabha events enriched by single final state–radiated photons, crossing the calorimeter barrel.The results are $\sigma_E = 16.4(2)$ MeV, $\sigma_{\Delta T} = 0.283(1)$ ns, $\sigma_{\rm Pt} = 13.2(3)$ MeV, $\sigma_{\rm Pz} = 8.9(1)$ MeV.

KLOE and HET acquisition systems are asynchronous. The DAΦNE radiofrequency signal, issued once per machine turn (325 ns), is independently recorded by the HET and KLOE for the synchronization. The HET acquisition system has been designed to register hits from more than two complete machine eturns.Figure 6, right panel, shows the common DAQ window of KLOE and HET. Any physics signal in coincidence is expected in that region while remaining buffer depth is used to evaluate the background directly from data.

Candidates of single-π^0 production from $\gamma\gamma$ scattering have been pre-filtered, recording information on hits in the tagger, trigger, DAΦNE operational parameters, clusters and tracks reconstructed in the central detector. Data are classified as single-arm (SA) or double-arm (DA) events. The DA data sample has been selected by requiring a time delay between the two stations corresponding to $|\Delta_{\rm e,p}| < 2$ bunch. This sample contains the HET-electron * HET-positron coincidences which are expected, from resolution studies, within 1 bunch. Contemporary a control sample with a time delay between the two stations $2 < \Delta_{\rm e,p} < 7$ bunches, has been selected large enough to perform a data-driven analysis to characterize the coincidences. The SA data sample has been selected by choosing events in time with the KLOE trigger and events in time with a bunch giving two clusters in KLOE with energy $20 < E_{\rm clu} < 300$ MeV and a time delay between the HET station and KLOE within 4 bunches. The number of expected $\gamma\gamma$ events is predicted by using the *EKHARA* MC generator [2], account for detector resolutions, together with the BDSIM package [3], a GEANT4 application which allows to track leptons along the machine optics. A total integrated luminosity of about 550 pb^{-1} has been analyzed. The background has been carefully evaluated on a run-by-run basis by using an “untagged” data sample containing events out of the coincidence between taggers and KLOE DAQ.

3 CED

If in 2016 we changed completely the data handling paradigm and the computing architecture, in 2017 we are picking up the results of that change. No inefficiency or delayed operations have been experienced: the storage worked without any faults or slow down failure and the data taking has been progressing without any interference with both data analysis and reconstruction.

The take over of NFS with GPFS and Ethernet with Fiber Channel made this improvement. The NFS network huge servers have been moved from their massive working point to a lightweight duty. Several new GPFS small servers took over the NFS old server duty and the efficiency was improved by a factor ten. The bandwidth data load presently feeds the number crunching servers without any stop driving our efficiency in terms of reconstructed data to an apex never reached before.

Disk array storage was increased with a new device which is the state of the art of the disk array market. Every byte is now available with a higher level of data safety and a very flexible storing method and can be used only when necessary. Presently storage overbooking avoids any resource waste: only the space in use is really allocated and no servers receive a disk full error while are working.

In view of the massive data reconstruction, activities to reduce the CPU load of the official reconstruction program started also exploiting the presence, for some months, of a student with an internship program with the VIA university in Denmark. A detailed analysis of the code architecture was done starting the revision of some million lines of code, written over the years by different generation of physicists. The languages used are Fortran, C and C++, and this clearly gives an idea of the effort required to identify the code weak points. The target is to decrease by a factor five or more, the total reconstruction time to be able to process data and obtain physics results much faster.

4 Physics achievements

4.1 U boson search: combined limit from $\mu\mu\gamma/\pi\pi\gamma$

The existence of an accessible portal to a hypothetical low-mass dark sector is among present hot topics of physics beyond the Standard Model searches. KLOE has already given a great contribution investigating the "visible" decays of the U-boson and published three searches for radiative U-boson production in the $e^+e^- \to U\gamma$, with the U-boson decaying into a pair of: i) muons, using a data sample of 240 pb^{-1} [4], ii) electrons, using a sample of 1.54 fb^{-1} [5], and iii) pions analyzing the whole KLOE data set corresponding to almost 2 fb^{-1} [6]. As conclusion of the work done on U-boson search by using the initial state radiation method, the $e^+e^- \to U\gamma_{\rm ISR}$, $U \to \mu^+\mu^-$ limit was updated increasing the statistics to the full KLOE data set.

Candidates of $\mu^+\mu^-\gamma$ events have been selected by requiring a small-angle ISR photon and two charged tracks with acceptance between 50° and 130°. Kinematical cuts together with the small-angle event selection allow to reduce the background coming from Final State Radiation and ϕ-resonant processes and to increase the sensitivity to U-boson signal [7]. At the end of the analysis chain residual backgrounds from $e^+e^- \to \phi \to \pi^+\pi^-\pi^0$ and $e^+e^- \to \ell^+\ell^-\gamma$ ($\ell = e, \pi$) ISR processes are at the level of few %. The new search confirms no U-boson signal in the di-muon invariant mass spectrum and a new 90% CL exclusion limit for the kinetic mixing parameter ε^2 has been set. The irreducible background $e^+e^- \to \mu^+\mu^-\gamma$ has been estimated directly from data with a fit to the side bands with Chebyshev polynomials while the limit extraction has been performed by using the Confidence Level Signal Technique [8], taking into account of the systematic error due to the background estimation (less the 1% in the most of the range).

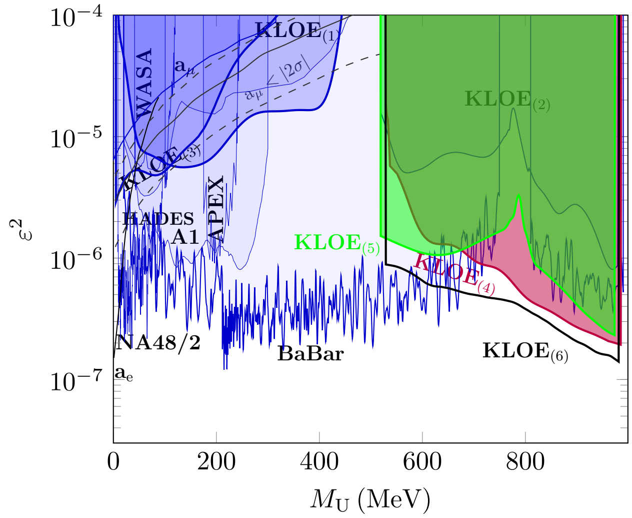

Figure 7: 90% CL exclusion plot for ε^2 as a function of the U-boson mass for $e^+e^- \to U\gamma$, $U \to \mu^+\mu^-$ with full KLOE statistics (green) and $\mu^+\mu^-\gamma\,/\pi^+\pi^-\gamma$ combined limit (black line) together with limits from the A1 [9] and APEX [10], the limits from the ϕ Dalitz dacay (KLOE$_{(1)}$) [11] and $\mathrm{e^+e^-} \to \mathrm{U}\gamma$ process where the U boson decays in $\mathrm{e^+e^-}$ or $\mu^+\mu^-$ or $\pi^+\pi^-$ (KLOE$_{(3)}$, KLOE$_{(2)}$ and KLOE$_{(4)}$ respectively) [5, 4, 6]; the WASA [15], HADES [16], BaBar [12] and NA48/2 [13].

The new muon limit is of the order of the existing ones ($\varepsilon^2 < 3 \times 10^{-6} - 2 \times 10^{-7}$), therefore, a combined limit has been extracted considering both $U \to \mu^+\mu^-\,, \pi^+\pi^-$ decays in the 500-1000 MeV mass region. The combination of the two decays reduces the loss of sensitivity which affects the muon channel in the $\rho - \omega$ region thanks to the dominant hadron branching fraction of the $U \to \pi^+\pi^-$ decay channel. The combined limit is more stringent of current set constraints in the U-boson mass range between 650 and 987 MeV. The preliminary $\mu^+\mu^-\gamma$ and the combined $\mu^+\mu^-\gamma/\pi^+\pi^-\gamma$ limits, presented at the EPS-HEP2017 conference [17], are shown in figure 7 together with the limits set by other experiments in the 0-1000 MeV U-boson mass range.

4.2 Combination of KLOE $\sigma(e^+e^- \to \mu^+\mu^-\gamma(\gamma))$ measurements and determination of $a_\mu^{\pi^+\pi^-}$ in the energy range $0.10 < s < 0.95$ GeV

The anomalous magnetic moment of the muon, a_μ, is one of the best known quantities in particle physics. The long standing deviation of more than $3\,\sigma$'s between its measured value and the Standard Model prediction motivates the improvement of both quantities. From the theory side, the limiting factor is presently the precision of the hadronic vacuum polarisation contribution (a_μ^{HVP}). At low energies, it cannot be calculated from perturbative QCD but has to be evaluated with a dispersion integral using measured hadronic cross sections.

KLOE preformed three precision measurements of the $\sigma(e^+e^- \to \mu^+\mu^-\gamma(\gamma))$ cross section using initial state radiation [18, 19, 20], providing an important input for the theoretical evaluation of a_μ^{HVP}. A re-analysis of these measurements has been performed in order to combine them while properly taking into account correlations for both statistical and systematic uncertainties. For both of them, full covariance matrices have been constructed. The result is reported in Fig. 8 left.

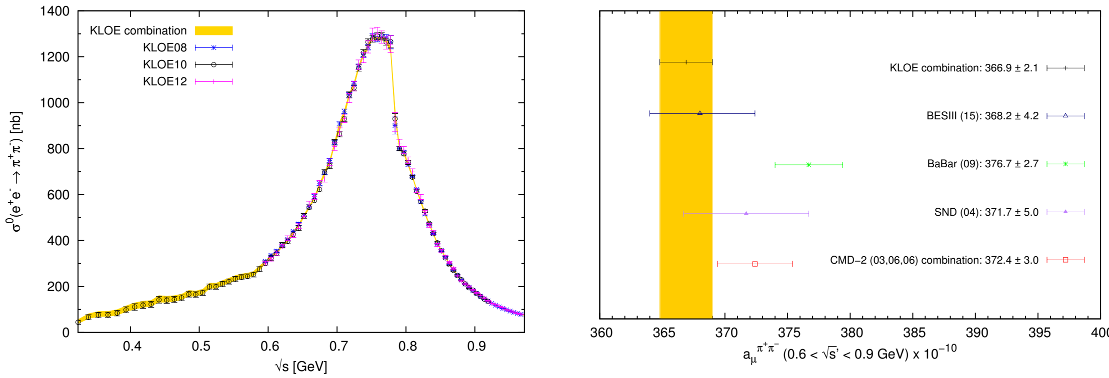

Figure 8: Left: cross section of the $e^+e^- \rightarrow \pi^+\pi^-$ process in the whole energy range covered by KLOE measurements. Right: $a_\mu^{\pi^+\pi^-}$ estimate from KLOE combination in the energy range $0.6 < \sqrt{s} < 0.9$ GeV, compared with values from other experiments.

The resulting anomalous magnetic moment of the muon in the full energy range is evaluated to be:

$$a_\mu^{\pi^+\pi^-(0.1\leq s\leq 0.95\mathrm{GeV}^2)=(489.8\pm 1.7_{\mathrm{stat}}\pm 4.8\mathrm{syst})\times 10^{-10}}. \tag{1}$$

In Fig. 8 right, KLOE combined result is compared with estimates from other experiments in the overlapping energy range.

4.3 K$_S$ semileptonic charge asymmetry

Pure K$_S$ samples have been selected identifying the K$_L$ interaction in the calorimeter (K$_L$-crash). In particular $K_S \rightarrow \pi e\nu$ decays are selected requiring a K$_L$-crash and two tracks forming a vertex close to the IP and associated with two energy deposits in the calorimeter. Pions and electrons are identified using their time of flight (TOF). A control sample of $\phi \rightarrow K_S K_L \rightarrow \pi^0\pi^0, \pi e\nu$ with the semileptonic decay close to the IP has been used to correct efficiencies evaluated with Monte Carlo. The analysis of 1.7 fb^{-1} of KLOE data yields a preliminary measurement of the K$_S$ semileptonic charge asymmetry of $A_S = (-3.9 \pm 5.7^{+3.3}_{-2.4})$x10^{-3} [21] improving by about a factor two the statistical uncertainty with respect to previous KLOE result [22]. The measured A$_S$ value is consistent with the expectation A$_S \simeq A_L$ 3.3x10^{-3} imposed by CPT invariance, with A$_L$ the K$_L$ semileptonic charge asymmetry precisely measured [23], and its uncertainty is approaching the level necessary to reveal CP violation with K$_S$ (i.e. A$_S \neq 0$).

Moreover a CPT test can be performed using the sum and the difference of A$_S$ and A$_L$. In fact using the values of A$_L$, Re(δ), and Re(ϵ) from other experiments [9], with ϵ and δ the parameters describing CP and CPT violation in the mixing of neutral kaons, the real part of the CPT violating and ΔS = ΔQ violating (conserving) parameter x$_-$(y) in semileptonic decay amplitudes can be evaluated: Re(x$_-$) = (A$_S$ - A$_L$)/4 - Re(δ) = (-2.1 ±1.6)x10^{-3} and Re(y)=Re(ϵ)-(A$_S$ + A$_L$)/4=(1.8 ±1.6)x10^{-3} improving the uncertainty with respect to previous results [22].

With the analysis of the full KLOE-2 data set, the uncertainty on A$_S$ can be further reduced at the level of $\sim$ 3x10^{-3}.

4.4 Testing CP with BR($K_S \to 3\pi^0$) upper limit with KLOE-2

The Standard Model prediction for the branching ratio of the CP-violating decay $K_S \to 3\pi^0$ is BR($K_S \to 3\pi^0$) $\sim 1.9\text{x}10^{-9}$, making the direct observation of this decay quite a challenge.

To improve present best upper limit on BR($K_S \to 3\pi^0$) $< 2.6\text{x}10^{-8}$ at 90% C.L. which was set with 1.7 fb^{-1} of KLOE data, searching for six photons coming from the IP and a K_L-crash [24], the Analysis with KLOE-2 data has started and will provide additional 5 fb^{-1}.

A preliminary analysis of 300 pb^{-1} presented at EPS-HEP 2017 conference shows the good quality of KLOE-2 data even in presence of a larger machine background with respect to KLOE. After hardening the selection criteria to get about ten times better background rejection and after applying the scheme of the previous analysis, only one candidate event survives, leaving room for improvements and the possibility to reach a final sensitivity on the BR below 10^{-8} [25].

References

1. PoS(EPS-HEP2017) 491
2. H. Czyz, S. Ivashyn, Comput. Phys. Commun. 182 (2011) 1338.
3. I. Agapov, G.A. Blair, S. Malton, L. Deacon, Nucl. Instrum. Meth. A 606 (2009) 708.
4. D. Babusci et al., Phys. Lett. B 736 (2014) 459.
5. A. Anastasi et al., Phys. Lett. B 750 (2015) 633 .
6. A. Anastasi et al., Phys. Lett. B 757 (2016) 356.
7. L. Barzè et al., Eur. Phys. J. C 71 (2011) 1680.
8. G. C. Feldman, R. D. Cousins, Phis. Rev. D 57 (1998) 3873.
9. H. Merkel, et al., Phys. Rev. Lett. 112 (2014) 221802.
10. S. Abrahamyan et al., Phys. Rev. Lett. 107 (2011) 191804.
11. D. Babusci, et al., Phys. Lett. B 720 (2013) 111-115.
12. J. P. Lees et al., Phys. Rev. Lett. 113, 201801 (2014).
13. J.R. Batley et al., Phys. Lett. B 746 (2015) 178.
14. M. Pospelov, Phys. Rev. D 80 (2009) 095002.
15. WASA-at-COSY Collaboration, P. Adlarson et al., Phys. Lett. B 726 (2013) 187.
16. G. Agakishiev et al., HADES Collaboration, Phys. Lett. B 731 (2014) 265.
17. PoS(EPS-HEP2017) 073
18. F. Ambrosino et al. [KLOE Collaboration], Phys. Lett. B 670 (2009) 285.
19. F. Ambrosino et al. [KLOE Collaboration], Phys. Lett. B 700 (2011) 102.
20. D. Babusci et al. [KLOE/KLOE-2 Collaborations], Phys. Lett. B 720 (2013) 336.
21. PoS (EPS-HEP2017) 213

22. F. Ambrosino et al., KLOE collaboration, Phys. Lett. B 636 (2006) 173.
23. C. Patrignani et al. (Particle Data Group), Chin. Phys. C 40, 100001 (2016).
24. D. Babusci et al., KLOE-2 collaboration, Phys. Lett. B 723, 54 (2013).
25. PoS (EPS-HEP2017) 213